Scalable Approaches for Copper Nanocrystal Synthesis under Ambient Conditions for Printed Electronics

Arnau Oliva-Puigdomènech,[†] Jonathan De Roo,[‡] Hannes Van Avermaet,[†,¶] Klaartje De Buysser,[§] and Zeger Hens*[,†,¶]

[†]*Physics and Chemistry of Nanostructures, Ghent University, Ghent, Belgium*

[‡]*Department of Chemistry, Basel University, Basel, Switzerland*

[¶]*Center for Nano and Biophotonics, Ghent University, Belgium*

[§]*Sol-gel Centre for Research on Inorganic Powders and Thin films Synthesis, Ghent University, Ghent, Belgium*

E-mail: zeger.hens@ugent.be

Abstract

We demonstrate the synthesis of copper nanocolloids by the thermal decomposition of copper formate in oleylamine under ambient conditions. By progressively increasing the loading of copper formate in the reaction mixture and imposing sufficiently high conversion rates, we demonstrate the formation of nanocrystals that are more than 97% pure copper without using an inert atmosphere. We attribute this result to the excess of copper formate relative to initially dissolved oxygen, and to the suppression of oxygen influx in the reactor. By adjusting the precursor and ligand concentrations, we obtain copper nanocrystals with sizes ranging from 10 to 200 nm. In view of applications, we show that the reaction can be upscaled to a 1 L reaction volume to produce over

50 grams of copper nanocrystals. Moreover, we formulate a conductive ink based on the copper nanocolloids obtained here with which we printed copper films exhibiting a resistivity of 23 $\mu\Omega \cdot$ cm after thermal sintering under N_2. We conclude that the approach presented here consititutes a next step towards the cost-effective production of metallic copper nanocrystals for printed electronics.

Introduction

Over the last decade, research interest in copper nanocrystals (Cu NCs) has increased due to the broad application potential of these materials in fields such as catalysis, sensing, optics and electronics.[1–5] In particular, copper is an excellent conductor and Cu NCs could replace silver NCs as the main constituent of conductive inks.[6–8] Such inks are of high interest for the printed electronics, which focuses on the fabrication of low-cost devices at high volumes, such as RFID tags.[8] While silver is a slightly better electrical conductor, copper is more abundant and considerably cheaper.[9] However, Cu is more prone to oxidation than silver, an issue that is exacerbated for nanometer-sized crystallites.[10] Since copper oxides are semiconductors rather than metals, oxidation suppression is critical when utilizing Cu NCs in conductive inks. Hence, the primary challenge to capitalize on the low cost of Cu for conductive inks is to develop an inexpensive synthesis that yields metallic Cu NCs,[11,12] and many literature reports have focused on the synthesis of such Cu NCs. These studies involve a broad range of synthesis methods, such as chemical reduction,[11,13,14] thermal decomposition,[15,16] micro-emulsion,[17,18] laser ablation,[19,20] or wire explosion.[21]

Among the different approaches to form Cu NCs, wet-chemical synthesis methods involving chemical reduction or thermal decomposition stand out due to their straightforward implementation and their offering a good control over the physical and chemical properties of the resulting NCs.[4,8] In the case of chemical reduction, strong reducing agents such as hydrazine,[22–26] or sodium borohydrate[13,27] are typically used to reduce copper salts, or the reaction is carried out under a hydrogen containing atmosphere.[28,29] The addition of such

reducing agents to a reaction mixture can lead to the formation of Cu NCs with a good control over the NC size and morphology, even at low temperature and under ambient conditions.[26,30,31] Moreover, by using surface active moieties such as oleic acid, Cu oxidation can be markedly suppressed.[32] However, the use of a hazardous reducing agent is a matter of concern for the large scale production of Cu NCs.

The synthesis of Cu NCs by the thermal decomposition of a copper precursor can be a convenient alternative to chemical reduction since no additional reducing agent is required. For example, Sun *et al.* first reported the thermolysis of metal formates in the presence of oleylamine and oleic acid to form metal and metal oxides NCs.[33] Other precursors, such as [bis(2-hydroxy-1-naphthaldehydato)copper(II)], [bis(salicylaldiminato)copper(II)] or copper oxalate were successfully used by Salavati-Niasari and co-workers to synthesize Cu NCs of different diameters.[15,34,35] Similarly, copper(II) 2-ethylhexanoate was employed by Kim *et al.* to form 70-80 nm Cu nanocolloids further shelled with copper formate to stall oxidation.[12] Alternatively, other researchers first synthesized copper oleate, which can be thermally decomposed into Cu NCs without adding extra stabilizers.[36]

In the above described syntheses, long alkylamines or carboxylic acids play a large role. These compounds form complexes with the copper precursors with a reduced decomposition temperature, and stabilize the resulting dispersion of Cu NCs in apolar solutions. Still, a general concern with thermal decomposition is the need of an inert atmosphere that is used to avoid oxidation during decomposition. Opposite from this general approach, Kim *et al.* described the formation of Cu NCs by reacting $CuCl_2$ with sodium oleate in aqueous solution.[37] While these authors claim that no inert gases are needed to prevent oxidation of the Cu NCs, the reaction described is carried out in sealed, evacuated pyrex tubes; conditions that limit scalability. Alternatively, Bhattacharjee and co-workers highlight that Cu NCs can be formded by decomposing copper malonate in the presence of oleylamine and triphenylphosphine, without using inert conditions.[38] While interesting, the approach required elevated temperature (240 °C) and long reaction times (1 hour), and no conclusive data on

the absence of oxides were provided. Next to these specific limitations, the described procedures only yielded low amounts of material per reaction volume. These limited solid loadings raise the production cost and limit the use of the otherwise promising thermal decomposition pathway to Cu NC synthesis to laboratory scale.

In this study, we present a straightforward, low-cost and high solid-loading synthesis of Cu NCs, based on the low-temperature decomposition of copper(II) formate in oleylamine or oleylamine/dodecane mixtures. Oleylamine is used to dissolve copper(II) formate and to stabilize the resulting copper nanocolloid. By saturating the reaction mixture with the precursor and steering the synthesis by adjusting the temperature profile, we achieved two significant benefits. First, we greatly increased the solid loading, *i.e.*, the amount of Cu NCs produced per volume of reaction, reaching levels exceeding 50 g/L. Second, we could avoid using a protective atmosphere to perform the reaction and produce ¿97% pure metallic Cu NCs under air. By adjusting the composition of the reaction mixture, the size of the Cu NCs formed could be tuned from 10 to 200 nm. Furthermore, we demonstrated that the method is scalable by performing a liter-scale demonstrator synthesis that effectively yields >50 grams of Cu NCs. Finally, an ink containing Cu NCs was formulated and deposited on a glass substrate. Sintering of the film at 400 °C for 1 hour resulted in Cu patterns featuring a conductivity of 23 $\mu\Omega \cdot$ cm, proving that the Cu NCs synthesized by this method can be effectively utilized as fillers in conductive inks.

Experimental Section

Chemicals. Copper(II) formate tetrahydrate (Alfa Aesar, 98%), oleylamine (Acros Tech, 80-90%), n-dodecane (Merck Millipore, ≤99%), diacetone alcohol (Sigma-Aldrich, ≤99%), disperbyk 180 (BYK), byk-333 (BYK).

Synthesis of Cu NCs. Copper nanocrystals were synthesized by revising a method originally introduced by Sun *et al.*[33] and adapted in recent publications.[39,40] A 10 mL solution

of copper(II) formate in an oleylamine:dodecane mixture was formed by heating the mixture at 60 °C until the copper(II) formate was fully dissolved. Unless mentioned otherwise, the temperature was raised to 140 °C in a constant heating rate of 10 °C/min and kept at this temperature for 10 minutes before cooling down. Cu NCs where extracted from the reaction mixture and further purified by repetitive precipitation/resuspension cycles using toluene as solvent and ethanol or methanol as non-solvent.

Structural Characterization. Transmission electron microscopy (TEM) images were recorded on a Cs-corrected JEOL 2200-FS TEM operated at 200 kV. X-ray diffraction (XRD) analysis was conducted on a Thermo Scientific ARL X'Tra diffractometer, operated at 40 kV/30 mA using Cu-Kα radiation (λ = 1.5406 Å) and a Peltier cooled Si(Li) solid-state detector. Scanning electron microscopy (SEM) images were recorded on a JEOL JSM-7600F Schottky Field Emission.

Rietveld refinement. The XRD data were collected on a Thermo Scientific ARL X'tra Diffractometer equipped with a Peltier cooled detector. Samples were measured in θ-2θ geometry over an angular range of $20 - 80°$ (2θ) (CuKα radiation) using a $0.02°$ 2θ step size and 1 s/step counting time. The Rietveld method for whole-powder pattern fitting was used and the Topas Academic V4.1 software was used for Rietveld refinement.[41] The refined parameters were the measurement specific or sample displacement error, a cosine Chebyshev function of 10 polynomial terms for background correction, phase specific scale factors, unit cell parameters and Lorentzian peak shape broadening parameters.

Ink formulation A washed and dry powder of Cu NCs was dispersed in diacetone alcohol (50% mass Cu loading), 1% disperbyk 180 and 0.3% byk 333, then the solution was sonicated for 1 hour to ensure full dispersion. The ink was deposited using a 6 μm wet thick film thickness wire bar coater. The samples were sintered in an oven under N_2 atmosphere at 400 °C for 1 hour. Thickness was determined by scratching a sample and measuring the step

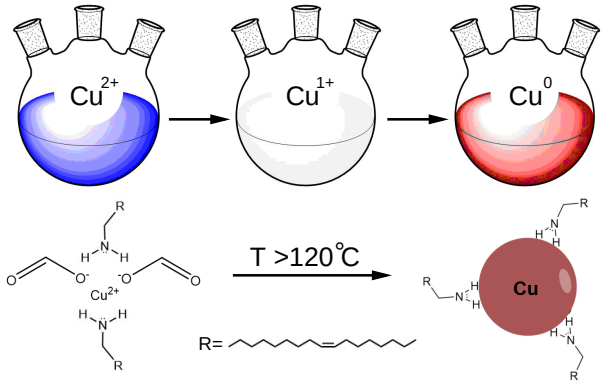

Scheme 1: Schematic depiction of the synthesis of Cu Nanocrystals.

height between sample and coating with a Taylor-Hobson Talystep mechanical profilometer. The square resistance was measured using a custom-build 4-point probe with equal spacing between probes. The absolute resistivity of the layers was calculated by multiplying the square resistance by the thickness and the correction factor.[42]

Results and discussion

Standard synthesis

As described in the Experimental Section, any synthesis described in this work starts with the formation of a 10 mL solution of copper formate ($Cu(HCO_2)_2$) in oleylamine ($OlNH_2$) and dodecane (see 1). Here, $OlNH_2$ is used as the complexing agent to bring the copper precursor in solution. Moreover, $OlNH_2$ is known to reduce the overall decomposition temperature of the $Cu(HCO_2)_2$:$OlNH_2$ complex, originally around 200 °C for pure $Cu(HCO_2)_2$, to only 120 °C.[43,44] Different hypotheses have been presented to explain this decrease in reduction temperature. Marchal *et al.* argued, for example, that the *in-situ* reduction mechanism of

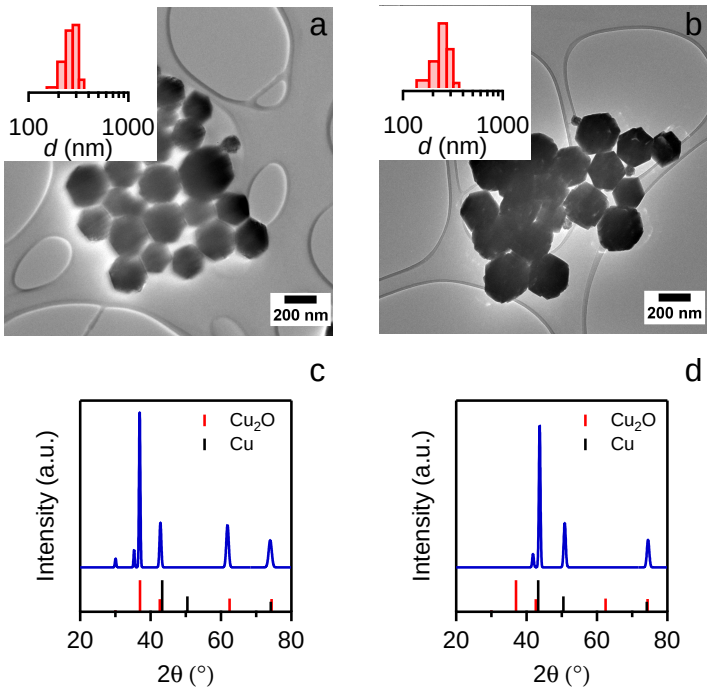

Figure 1: Low-resolution, brightfield TEM image of a: 2 g/L, 2:1 $OlNH_2$:$Cu(HCO_2)_2$ synthesis of Cu NCs under (a) ambient and (b) nitrogen atmosphere; (insets) Size histograms determined based on the analysis of 200 NCs in TEM images. XRD pattern of pristine NCs synthesized under (c) ambient and (d) nitrogen atmosphere. The mixture for the synthesis under nitrogen was degassed prior to the reaction.

copper formate proceeds *via* a transient Cu(I) intermediate.[45] Compared to other Cu(II) complexes, it was inferred that the decrease on the $Cu(HCO_2)_2$ reduction temperature arose from the low stability of the Cu(I) intermediate and the structural differences between Cu(II) and Cu(I) species along the thermal decomposition route. Such a two step decomposition has indeed been confirmed for the synthesis of Cu NCs from $Cu(HCO_2)_2$ used here,[40] where the reduction from Cu(II) to Cu(I) makes the originally blue reaction mixture turn pale at 120 °C. By furthering increasing the reaction temperature, this step is followed by the subsequent reduction of Cu(I) to Cu(0), which precipitates to form Cu NCs that yield a dark-red/brown reaction mixture. The conversion yield of $Cu(HCO_2)_2$ to metallic Cu was estimated before at $\sim 65\%$, and the resulting NCs were shown to feature a surface capping of $OlNH_2$, which stabilizes the nanocolloid by steric hindrance.

Figure 1 presents the main characteristics of the products obtained from the decompo-

sition of a $Cu(HCO_2)_2$ solution containing 2 g/L of Cu and featuring a 2:1 molar ratio of $OlNH_2$: $Cu(HCO_2)_2$, either synthesized under ambient (Figure 1a) or inert atmosphere (Figure 1b). As can be seen, these specific synthesis conditions lead to a polydisperse distribution of NCs, with an average size of 240 ± 40 nm and 280 ± 150 nm, with no noticeable impact of the synthesis environment on the morphology. One sees that in both cases, the NCs exhibit a projected hexagonal shape, suggesting that the crystallites are cuboctahedrons.[14,46] The fact that such large NCs maintain a cuboctahedral shape points towards a similar growth rate of both (100) and (111) facets, suggesting a non-preferential binding of $OlNH_2$ to either facet.[47,48] Despite the similar morphology, a very different crystallographic structure is obtained depending on the synthesis atmosphere. As can be seen in Figure 1c, the X-ray diffraction pattern of NCs synthesized under ambient conditions corresponds to that of Cu_2O (JCPDS 05-0667) and features a diffraction peak characteristic of the (111) lattice plane of CuO at 38.75° (JCPDS 80-1268). The formation of copper oxide is not unexpected since an inert atmosphere is typically used to prevent oxidation during the formation of Cu NCs.[16] On the other hand, the NCs obtained through a synthesis performed under inert conditions exhibit the X-ray diffraction pattern of metallic Cu^0 in its cubic structure (JCPDS 04-0836), confirming that formate and $OlNH_2$ can fully reduce Cu^{2+} to Cu^0 under inert conditions without the addition of an extra reducing agent.[49]

Oxidation Suppression During Cu Nanocrystal Synthesis: The Impact of Initially Dissolved Oxygen

Inspired by reports on the enhanced stability of copper nanocrystals synthesized in the presence of alkylamines,,[29] we aimed at defining synthesis conditions for which metallic Cu NCs are formed under ambient. In principle, oxidation suppression would require us to strictly avoid exposure to oxygen at all stages of the synthesis. As a first oxygen source, we considered all oxygen initially dissolved in the $OlNH_2$-dodecane solvent mixture at the start of the reaction. In chemical laboratories, it is common practice to protect oxygen-sensitive com-

pounds during a reaction by degassing the initial reaction mixture under vacuum. However, degassing is a time-consuming process that is impractical for large volumes. Moreover, if a reaction under ambient atmosphere is envisaged, initial degassing seems futile since oxygen can dissolve back into the solvent prior to the reaction.

To assess the impact of dissolved oxygen on the formation of Cu NCs, we estimated the concentration of dissolved oxygen in the initial $OlNH_2$-dodecane solvent mixture. According to published data,[50] the solubility of oxygen in *n*-dodecane amounts to 54.9 mg/L at 35 °C and atmospheric pressure. Using that value, we calculated that for the 2 g/L synthesis described in the previous section, the molar ratio between Cu formate and dissolved O_2 amounts to ∼18. To interpret the consequence of such an equivalence, we considered the formation of Cu_2O from Cu and O_2:

$$4Cu(s) + O_2(sol) \rightleftharpoons 2Cu_2O(s) \quad (1)$$

According to Equation 1, 4 moles of Cu are oxidized by 1 mole of O_2. Therefore, a sizable fraction of about 20% of the reduced copper could be re-oxidized by the oxygen initially dissolved in the reaction mixture of that 2 g/L synthesis. This suggests that further increasing the $Cu(HCO_2)_2$ concentration in the reaction mixture could be an efficient strategy to suppress oxidation. Indeed, such reaction mixtures would have an increased initial Cu/O_2 ratio and, consequently, a smaller fraction of re-oxidized Cu as a final product. For example, an increase of the Cu content to 40 g/L could decrease the expected fraction of re-oxidized copper to less than 1% of the total amount of Cu formed. Using such an approach, the initial oxidation of this small amount of Cu may lead to an oxygen-free reaction mixture; a *self-cleaning* effect that creates the inert environment necessary for the formation of metallic Cu NCs.

We tested the possible occurrence of this self-cleaning of the reaction mixture by running the $Cu(HCO_2)_2$ decomposition under ambient conditions in reaction mixtures with a different

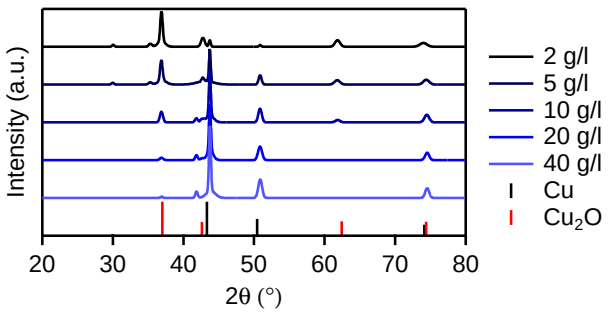

Figure 2: XRD patterns of Cu NCs synthesized with different concentrations of Cu without protective atmosphere. The molar ratio of $OlNH_2$:$Cu(HCO_2)_2$ has been kept at 2:1 and the heating rate at 20 °C/min for all syntheses. The NCs were purified and dried in ambient conditions prior to measurement.

Table 1: Copper ratios extracted from Rietveld refinement analysis of the XRD data from Figure 2.

[Cu]	Cu (%)	Cu_2O(%)
2 g/L	8.8 ± 0.5	91.2 ± 0.5
5 g/L	43.9 ± 0.5	56.1 ± 0.5
10 g/L	73.5 ± 0.6	26.5 ± 0.6
20 g/L	92.7 ± 0.7	7.3 ± 0.7
40 g/L	97.3 ± 0.6	2.7 ± 0.6

solid loading. Figure 2 presents XRD patterns of NCs obtained by $Cu(HCO_2)_2$ decomposition, for Cu loadings increasing from 2 to 50 g/L. As can be seen, the initial concentration of the copper precursor has a large impact on the extent of copper oxide formation. At low precursor concentration, the NCs mainly consist of Cu_2O. When using a solid loading of 2 g/L, the XRD pattern obtained closely resembles the one presented in 1c. However, as the concentration of the initial precursor is increased, the crystallographic phases gradually shift from Cu_2O to Cu. Table 1 summarizes the results of a Rietveld refinement of these diffractograms, which indicate that the metallic Cu content increases from 8.8% to 97.3% by increasing the concentration from 2 g/L to 40 g/L. Note that an oxidized fraction of about 2% for the 40 g/L synthesis is close to the estimated value based on the room temperature solubility of oxygen in *n*-dodecane. As an additional benefit, a larger concentration of precursor results in a higher amount of material produced per volume of reaction; synthesis

conditions that reduce the overall cost of producing Cu NCs and limit the generated waste.

Oxidation Suppression During Cu Nanocrystal Synthesis: Oxygen Intake During Synthesis

Apart from the initially dissolved oxygen, the influx of oxygen from the ambient surroundings can be a second oxygen source in an open reaction vessel, which we succinctly describe as a transition from gaseous to dissolved oxygen:

$$O_{2(g)} \rightleftharpoons O_{2(sol)} \tag{2}$$

This process will counteract the removal of oxygen in the reaction mixture by the oxidation of Cu^0 as described by Eq 1. Hence, to prevent further formation of copper oxide, the influx of oxygen in the reaction mixture should be restricted during the decomposition of the precursor and the nucleation and growth of Cu NCs. However, the flask cannot simply be sealed to block any gas inflow since the decomposition of $Cu(HCO_2)_2$ releases water, carbon dioxide and hydrogen according to the net chemical reaction:[43]

$$Cu(HCO_2)_2 \cdot 4H_2O_{(sol)} \rightarrow Cu_{(s)} + H_{2(g)} + 2CO_{2(g)} + 4H_2O_{(g)} \tag{3}$$

Clearly, such gas evolution would result in a problematic pressure increase in a closed flask.

To evaluate the impact of oxygen intake on the reaction, we started from the idea that the flow of gasses released from the reaction mixture by the decomposition of $Cu(HCO_2)_2$ can reduce or impede the influx of oxygen in the reaction vessel. Indeed, considering that the reaction occurs in an open flask exposed to ambient atmosphere, the total pressure in the headspace must remain constant. When the decomposition of $Cu(HCO_2)_2$ starts, evaporation of water and the generation of hydrogen and carbon dioxide from the solution increase the partial pressure of such gases above the liquid and decrease the oxygen partial

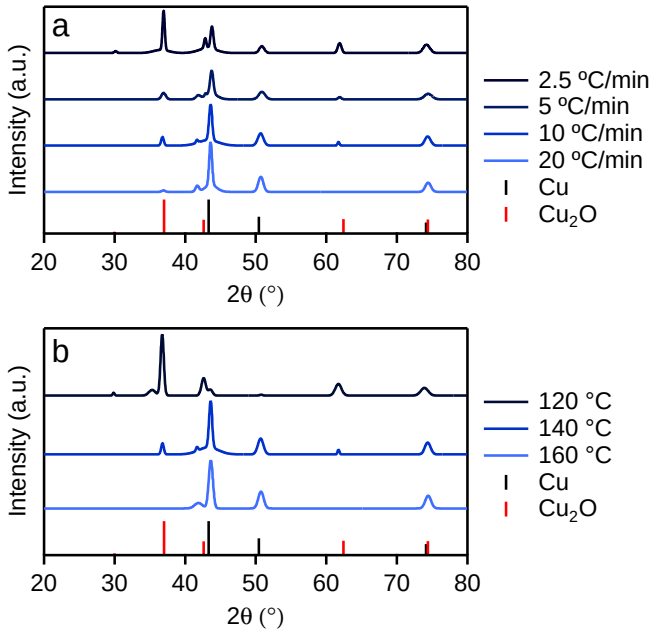

Figure 3: (a) XRD patterns of Cu NCs synthesized at different heating rates without protective atmosphere, to a final temperature of 140 °C. (b) XRD patterns of Cu NCs synthesized without protective atmosphere, at 10 °C/min to different final temperatures and held at these temperature for 10 min. The concentration of copper was set at 20 g/L and the molar ratio of $OlNH_2$:$Cu(HCO_2)_2$ 2:1 for all syntheses. The NCs were purified and dried in ambient conditions prior to characterization.

Table 2: Copper ratios extracted from Rietveld refinement analysis of the XRD data from Figure 3a.

Heating rate (°C/min)	Cu (%)	Cu_2O(%)
2.5	43.5 ± 0.7	56.5 ± 0.7
5	77.6 ± 1.2	22.4 ± 1.2
10	82.5 ± 0.8	17.5 ± 0.8
20	92.4 ± 1.6	7.6 ± 1.6

pressure to keep the total pressure constant. Importantly, this analysis suggests that the formation of such an oxygen-poor atmosphere in the reaction vessel will strongly depend on the reaction rate, where slow reactions will have hardly any impact, whereas fast reactions may strongly influence oxygen redissolution.

We evaluated the impact of the reaction rate on the formation of copper and copper oxide during $Cu(HCO_2)_2$ decomposition by either changing the rate at which the a final

Table 3: Copper ratios extracted from Rietveld refinement analysis of the XRD data from Figure 3b.

Final temperature (°C)	Cu (%)	Cu_2O(%)
120	8.5 ± 0.7	91.5 ± 0.7
140	82.5 ± 0.8	17.5 ± 0.8
160	90.1 ± 4.4	9.9 ± 4.4

reaction temperature of 140 °C is reached, or by changing that reaction temperature. Figure 3 represents the X-ray diffractograms recorded on the reaction product obtained for these different syntheses, which point towards an increased copper oxide content for slower heating rates or lower reaction temperatures, *i.e.*, conditions in which the overall reaction rate is lower. This qualitative picture is confirmed by a Rietveld analysis, the results of which are summarized in Tables 2 and 3. One sees that at the lowest heating rate used, a mixed copper/copper oxide product is obtained whereas a heating rate of 20 °C/min leads to a NC product consisting for ∼92% of Cu^0. Note that the latter result is in close agreement with the data listed in Table 1 for the same precursor concentration. Similarly, Table 3 indicates that changing the reaction temperature from 120 °C to 160 °C induces a shift of the end product composition from 90% copper oxide to 90% copper. Hence, we conclude that a lower reaction rate strongly facilitates the formation of copper oxide, probably by enabling influx and redissolution of oxygen from the surrounding atmosphere in the reaction mixture. On the other hand, high reaction rates can effectively suppress the redissolution of oxygen, which lead to an oxygen-poor reaction mixture in which Cu NCs can be formed, even under ambient conditions.

Size-Tuning During Cu Nanocrystal Synthesis

The size of Cu NCs is an important characteristic of a conductive ink based on a copper nanocolloid. For example, NCs with sizes larger than 50 nm can clog the nozzles of an ink-jet printer. On the other hand, smaller NCs have a larger surface-to-volume ratio. As a result,

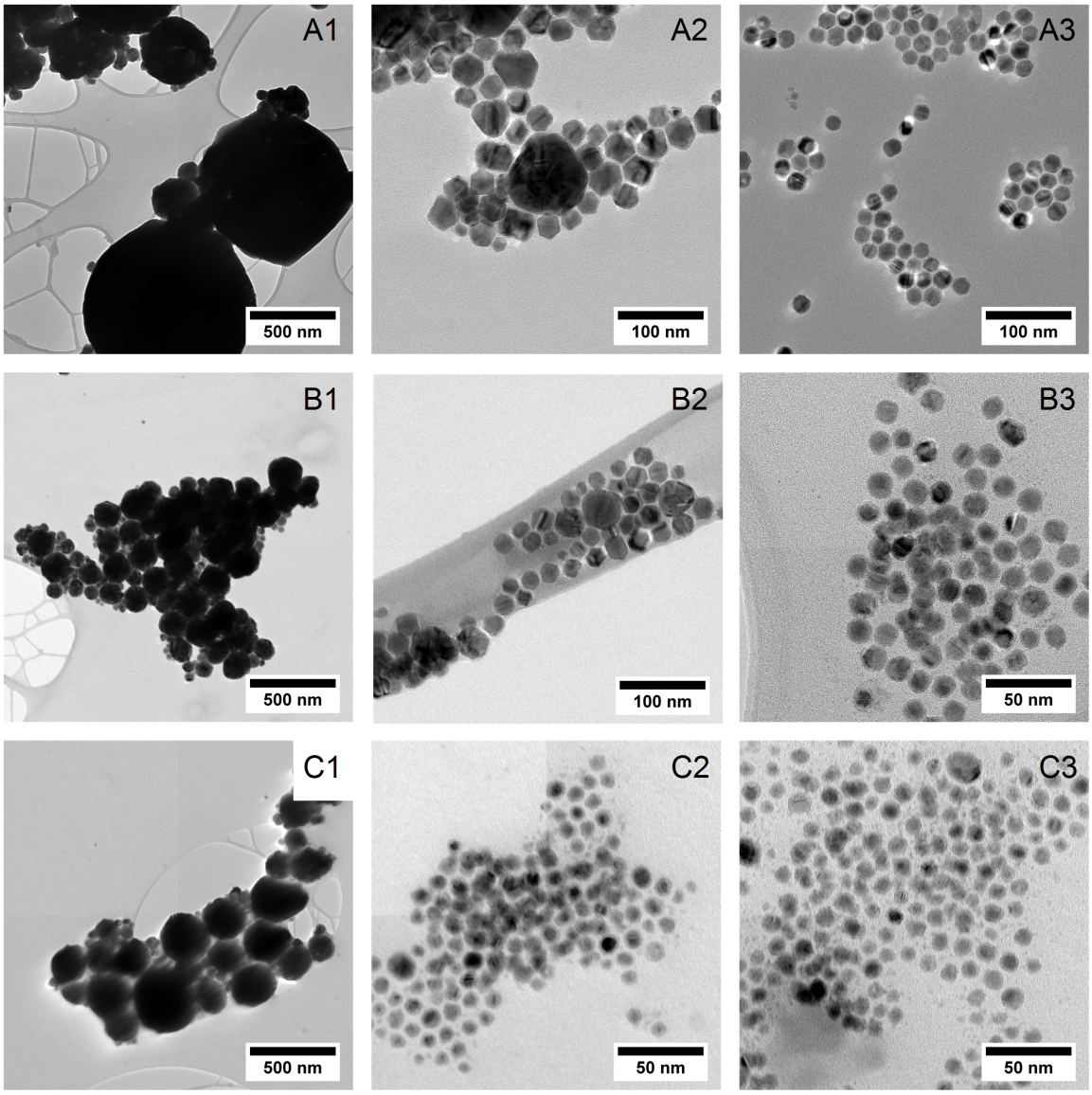

Figure 4: Low-resolution, brightfield TEM images of Cu NCs synthesized by means of adaptation to the standard synthesis, involving (A-C) different concentrations of copper [(A) 10 g/L; (B) 20 g/L; (C) 40 g/L] and (1-3) different $OlNH_2$:copper formate molar ratios [(1) 1:1; (2) 2:1; (3) 3:1]. All reactions are carried out using the standard protocol described in the Experimental Section, including a 10 mL reaction volume, a 10 °C/min heating rate, a final reaction temperature of 140 °C and a reaction time of 10 min.

an increasing amount of organic ligands is needed to stabilize a conductive ink, which can limit the solid loading.[51] For these reasons, a synthesis method that enables the nanocrystal size to be varied by minimal changes to the composition of the reaction mixtures is of high interest. To obtain such a level of control, we explored the influence of the reagent ratios,

Table 4: Particle size and standard deviation of the Cu NCs from Figure 4. Sizes are determined based on the analysis of 200 NCs in the images.

[Cu]	$OlNH_2$:$Cu(HCO_2)_2$		
	1:1	2:1	3:1
10 g/L	197.6 ± 182.8 nm	34.1 ± 16.9 nm	19.3 ± 2.9 nm
20 g/L	100.9 ± 54.4 nm	27.2 ± 9.2 nm	13.7 ± 1.3 nm
40 g/L	107.6 ± 85.3 nm	10.0 ± 1.4 nm	9.4 ± 1.4 nm

most notably the $OlNH_2$:$Cu(HCO_2)_2$ equivalence and the $Cu(HCO_2)_2$ concentration, on the reaction outcome while keeping other relevant parameters such as heating rate, synthesis time and reaction temperature constant. This approach is inspired by literature results on the synthesis of CdSe NCs, where both the reaction rate and the surfactant concentration proved useful variables to tune the resulting nanocrystal size.[52]

Figure 4 and Table 4 present the different nanocrystal sizes we obtained in this study, where we modified the $OlNH_2$ equivalence (left to right) or changed the $Cu(HCO_2)_2$ concentration (top to bottom) as compared to the standard synthesis as described in the Experimental Section. As can be seen, a low concentration of $OlNH_2$ concurs with the formation of large NCs, whereas a high ligand concentration leads to small NCs. These results confirm the observation made by Dai *et al.*[39] In the case that the $OlNH_2$: $Cu(HCO_2)_2$ equivalence is further increased to 8, the particle size is reduced down to 4 nm; a result in line with results we published previously.[40] Hence, we find that in the Cu NC synthesis used here, higher $OlNH_2$ concentrations induce a more pronounced nucleation event that leads to more, yet smaller NCs at the end of the reaction. Such a trend is different from what is often found in semiconductor NC synthesis, where larger ligand concentrations promote nanocrystal growth, thereby limiting nucleation and resulting in larger NCs.[53] Possibly, the reverse effect of ligand concentration on NC size observed here reflects the impact of ligand concentration on the size of Cu NCs reflects the lower growth rate of facets covered with a high surface density of ligands. It is also noteworthy that lower ligand concentration yield broader size distributions, a relation that complicates the determination of the average NC

size. For instance, using 1 equivalent of $OlNH_2$ yields an end product in which the NC diameter varies between 20 and 400 nm. The difference in particle growth can be linked to the solubility of $Cu(HCO_2)_2$, which only dissolves in non-polar solvents by complexation with $OlNH_2$. Since Cu^{2+} can be 6-fold coordinated, the 1 equivalent reaction mixture will comprise $Cu(HCO_2)_2$ complexed by 0,1 or 2 $OlNH_2$ ligands. Possibly, this diversity leads to a heterogeneous mixture in which $Cu(HCO_2)_2$ reacts at different rates and NCs with a broad range of sizes are formed.

Similarly, the initial concentration of $Cu(HCO_2)_2$ in the reaction mixture has an effect on the nanocrystal size. In that case, we find that a lower concentration of copper precursor in the reaction mixture leads to larger NCs, as can be seen in Figure 4 and Table 4 from top to bottom. This relation between NC size and precursor concentration is in line with previous results on the formation of CdSe NCs.[52] In that study, the link between higher precursor concentration and larger NCs was assigned to the underlying relation between the reaction rate and the NC size, where more rapid reactions promote nucleation over growth and lead to the formation of more, albeit smaller NCs.

Application Testing, Large Scale Synthesis and Electrical Resistivity of Printed Cu Films

To test the relevance of the proposed method to form Cu NCs, we carried out the reaction as described in the Methods section at a 1 L scale. To achieve this, we loaded 1 L of a one equivalent reaction mixture – containing 1 mole of $Cu(HCO_2)_2$ and 1 mole of $OlNH_2$ in dodecane – in an open 3 L flask. Referring to Figure 4, we expect that such conditions will yield 100 nm large Cu NCs, crystallite sizes well-suited for screen printing, while further enhancing the solid loading to 63 g/L. After vigorously stirring this reaction mixture with a mechanical stirrer at 50 °C, we raised the temperature to 140 °C to let Cu NCs form for 10 minutes. Afterwards, the reaction mixture was cooled down and purified using toluene as the solvent and ethanol as the non-solvent and decanting the supernatant after centrifugation.

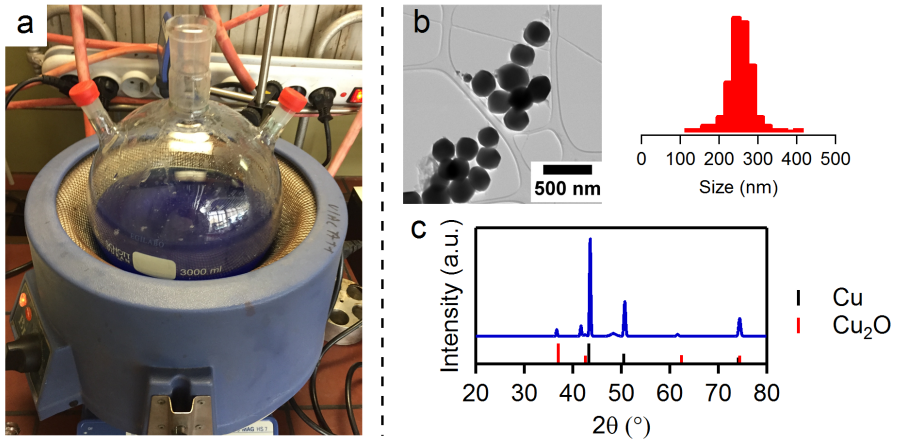

Figure 5: (a) Initial solution mixture prior to large-scale synthesis. An open 3 L round-bottom flask was used as vessel and a corresponding heating mantle was used as heating method. (b) Low resolution, brightfield TEM image of Cu NCs synthesized at 1M $Cu(HCO_2)_2$ concentration and 1M $OlNH_2$ in a 1 L volume. Average particle diameter was determined by sizing of 100 different particles. (c) XRD diffractogram of a washed powder sample, showing mainly presence of crystalline Cu and a minor presence of Cu_2O.

The washed powder we thus obtained was characterized via TEM and XRD. As shown in Figure 5b and 5c, this synthesis yielded NCs with an average diameter of 240 ± 39 nm, a larger average size and a more narrow size distribution than the NCs synthesized under similar conditions in a lab scale setup (see Figure 4). We attribute the difference in particle size to the larger reaction volume, which caused a decrease in the heating rate of the solution to approximately 3 °C/min. A slower heating rate induced a slower reaction, which implies that nucleation is suppressed relative to growth events such that larger NCs are obtained.[54] Also in this case, the XRD pattern of the reaction product shown in Figure 5c indicates that the synthesis yields a mixture of Cu and Cu_2O, albeit dominated by metallic copper. Based on a Rietveld analysis, we estimate that the reaction product consists for 92% of Cu and 8% of Cu_2O. Note that this outcome is in line with the results shown in Table 1 and Table 1, where the increased Cu_2O formation caused by the lower heating rate is partially offset by the higher copper loading.

In a second set of experiments, we synthesized Cu NCs by running a similar 1 equivalent, 1 M reaction as described above at a 100 mL scale. The reaction mixture was first stirred

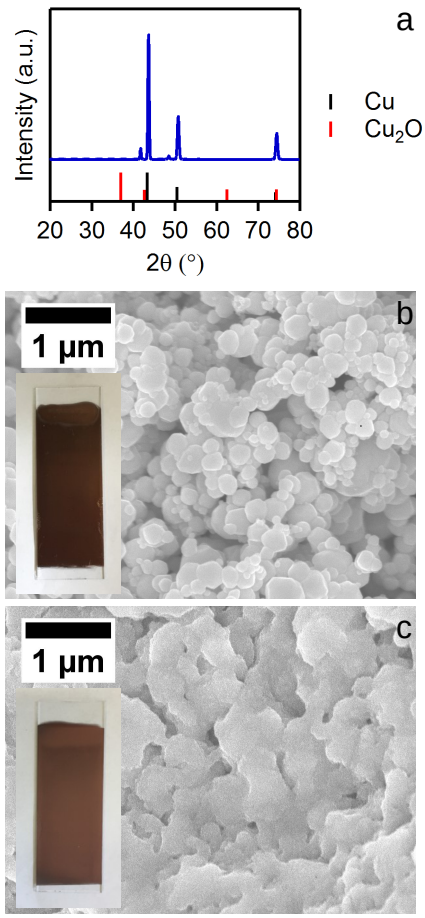

Figure 6: (a) XRD pattern of Cu NCs synthesized at 1M $Cu(HCO_2)_2$ concentration and 1M $OlNH_2$ in a 100 mL volume. Scanning electron microscope (SEM) image of Cu NCs films (b) before and (c) after sintering at 400 °C. Insets: Optical pictures of the films before and after sintering.

for 1 hour at 50 °C to dissolve $Cu(HCO_2)_2$, after which that reaction temperature was raised to 140 °C at a rate of 10 °C/min in ambient atmosphere. The mixture was held at this temperature for 10 min, cooled down and washed 3 times with toluene as the solvent and ethanol as the non-solvent. This resulted in $\sim$ 6 g of reaction product, which corresponds to a conversion yield of $\sim$ 95%. Figure 6a shows the x-ray diffractogram of the purified reaction product, which corresponds according to Rietveld analysis to 98.5% pure Cu. In a second step, a dried powder of these Cu NCs (50% in weight) was added to a solution of diacetone alcohol, disperbyk 180 (1%) – a dispersing additive – and byk 333 (0.3%) - a wetting agent - and sonicated for 1 hour to ensure full dispersion. The resulting paste was

deposited on a substrate and uniformally spread using a wire bar coater. Afterwards, the ink was dried under ambient atmosphere for 30 minutes before sintering. The dried layer was placed in a nitrogen-filled oven at 400 °C for 1 hour. The heat treatment resulted in the sintering of the Cu NCs as can be seen in the SEM images shown in Figure 6b (before) and Figure 6c (after). The sintered layer had a thickness of $1.8 \pm 0.2\,\mu$m (see Experimental Section), a reasonable number given the copper loading in the ink and the wet layer thickness of 6 μm, and an electrical resistivity as measured using a 4-point probe of 28 mΩ. Hence, the resulting layer featured an absolute resistivity of 23 $\mu\Omega \cdot$ cm, which corresponds to $\sim$ 7% of the conductivity of bulk Cu. While sintering at 400 °C seems prohibitively large for printed electronics applications, more local heating methods with a significantly lower thermal budget been proposed for sintering films of Cu NCs.[55–57] Clearly, such methods could be applied to the layers formed here as well.

Conclusion

Different reports in the literature showcased the possibility to synthesize copper metal nanocolloids under ambient conditions.[26,30,31] In view of applications in printed electronics, these approaches focused on high concentration reaction mixtures, reporting copper loadings in between 20 and 40 g/L,[26,31] and reported the formation of copper films with conductivities in the range $15 - 30\,\mu\Omega \cdot$ cm.[26,31] The reduction of the initial Cu(II) salts to metallic Cu(0), however, is achieved by means of strong reducing agents, such as hydrazine hydrate. While hydrazine hydrate most likely helps suppressing the formation of copper oxide during synthesis, the use of such a hazardous compound questions large scale production of copper nanocolloids using such a reducing agent. Less hazardous approaches based on the thermal decomposition of a copper precursor such as copper formate have been proposed recently, yet solid loadings are smaller and oxidation is prevented by carrying out all reaction steps under nitrogen.[39]

Here, we showed that copper oxidation during a reaction based on the thermal decomposition of a copper precursor can be kinetically suppressed. Enhancing the solid loading to 40 g/L shifts the equivalence between copper and dissolved oxygen such that 97% pure metallic copper can be obtained when the reaction is carried out at a rate that outpaces the influx of oxygen in the reaction mixture from the surroundings. Interestingly, since the copper/dissolved oxygen equivalence will be independent of reactor design or reaction volumes, the reaction rates used here can be used as a benchmark when implementing the approach in a different setup. Moreover, we find that straightforward adaptations of the reaction conditions enable copper nanocrystals to be synthesized with sizes ranging from a few to a few hundreds of nanometers, a tuning that is essential to adjust a conductive ink to the printing method of choice. Finally, we showed that the same oxidation suppression approach can be carried out at liter scale to produce 50 g/L of Cu nanocrystals and that conductive inks can be formulated using Cu NCs formed by this method. After thermal synthesis, printed Cu films are obtained with a resistivity of 23 $\mu\Omega \cdot$cm. Being comparable to previously published figures,[58,59] including methods where copper nanocolloids were synthesized under ambient with hydrazine hydrate,[26,31] such a conductivity highlights the potential of utilizing copper nanocolloids *via* the described method for printed electronics applications.

Acknowledgement

Z.H. acknowledges SIM-Flanders for supporting this research through the SIM-ICON Met@link.

References

(1) Wang, Z.; Chen, B.; Rogach, A. L. Synthesis, Optical Properties and Applications of Light-Emitting Copper Nanoclusters. *Nanoscale Horiz.* **2017**, *2*, 135–146.

(2) Ramani, T.; Leon Prasanth, K.; Sreedhar, B. Air Stable Colloidal Copper Nanoparticles: Synthesis, Characterization and their Surface-Enhanced Raman Scattering Properties. *Phys. E Low-Dimensional Syst. Nanostructures* **2016**, *77*, 65–71.

(3) Zhang, P.; Sui, Y.; Wang, C.; Wang, Y.; Cui, G.; Wang, C.; Liu, B.; Zou, B. A One-Step Green Route to Synthesize Copper Nanocrystals and their Applications in Catalysis and Surface Enhanced Raman Scattering. *Nanoscale* **2014**, 5343–5350.

(4) Gawande, M. B.; Goswami, A.; Felpin, F. X.; Asefa, T.; Huang, X.; Silva, R.; Zou, X.; Zboril, R.; Varma, R. S. Cu and Cu-Based Nanoparticles: Synthesis and Applications in Catalysis. *Chem. Rev.* **2016**, *116*, 3722–3811.

(5) Siwach, O. P.; Sen, P. Synthesis and Study of Fluorescence Properties of Cu Nanoparticles. *J. Nanoparticle Res.* **2008**, *10*, 107–114.

(6) Kang, J. S.; Kim, H. S.; Ryu, J.; Thomas Hahn, H.; Jang, S.; Joung, J. W. Inkjet Printed Electronics Using Copper Nanoparticle Ink. *J. Mater. Sci. Mater. Electron.* **2010**, *21*, 1213–1220.

(7) Tsai, C.-Y. Y.; Chang, W.-C. C.; Chen, G.-L. L.; Chung, C.-H. H.; Liang, J.-X. X.; Ma, W.-Y. Y.; Yang, T.-N. N. A Study of the Preparation and Properties of Antioxidative Copper Inks with High Electrical Conductivity. *Nanoscale Res. Lett.* **2015**, *10*, 357.

(8) Magdassi, S.; Grouchko, M.; Kamyshny, A. Copper Nanoparticles for Printed Electronics: Routes Towards Achieving Oxidation Stability. *Mater. (Basel).* **2010**, *3*, 4626–4638.

(9) Kamyshny, A.; Magdassi, S. Conductive Nanomaterials for Printed Electronics. *Small* **2014**, *10*, 3515–3535.

(10) Rice, D. W. Atmospheric Corrosion of Copper and Silver. *J. Electrochem. Soc.* **1981**, *128*, 275.

(11) Lee, Y.; Choi, J.-r. R.; Lee, K. J.; Stott, N. E.; Kim, D. Large-Scale Synthesis of Copper Nanoparticles by Chemically Controlled Reduction for Applications of Inkjet-Printed Electronics. *Nanotechnology* **2008**, *19*, 415604.

(12) Kim, I.; Kim, Y.; Woo, K.; Ryu, E.-H.; Yon, K.-Y.; Cao, G.; Moon, J. Synthesis of Oxidation-Resistant Core–Shell Copper Nanoparticles. *RSC Adv.* **2013**, *3*, 15169.

(13) Lisiecki, I.; Billoudet, F.; Pileni, M. P. Control of the Shape and the Size of Copper Metallic Particles. *J. Phys. Chem.* **1996**, *100*, 4160–4166.

(14) Salzemann, C.; Lisiecki, I.; Urban, J.; Pileni, M. P. Anisotropic copper nanocrystals synthesized in a supersaturated medium: Nanocrystal growth. *Langmuir* **2004**, *20*, 11772–11777.

(15) Salavati-Niasari, M.; Mir, N.; Davar, F. A Novel Precursor for Synthesis of Metallic Copper Nanocrystals by Thermal Decomposition Approach. *Appl. Surf. Sci.* **2010**, *256*, 4003–4008.

(16) Mott, D.; Galkowski, J.; Wang, L.; Luo, J.; Zhong, C. J. Synthesis of Size-Controlled and Shaped Copper Nanoparticles. *Langmuir* **2007**, *23*, 5740–5745.

(17) Solanki, J. N.; Sengupta, R.; Murthy, Z. V. P. Synthesis of Copper Sulphide and Copper Nanoparticles with Microemulsion Method. *Solid State Sci.* **2010**, *12*, 1560–1566.

(18) Ahmed, J.; Ramanujachary, K. V.; Lofland, S. E.; Furiato, A.; Gupta, G.; Shivaprasad, S. M.; Ganguli, A. K. Bimetallic Cu-Ni Nanoparticles of Varying Composition ($CuNi_3$, CuNi, Cu_3Ni). *Colloids Surfaces A Physicochem. Eng. Asp.* **2008**, *331*, 206–212.

(19) Saito, M.; Yasukawa, K.; Umeda, T.; Aoi, Y. Copper Nanoparticles Fabricated by Laser Ablation in Polysiloxane. *Opt. Mater. (Amst).* **2008**, *30*, 1201–1204.

(20) Muniz-Miranda, M.; Gellini, C.; Giorgetti, E. Surface-Enhanced Raman Scattering from Copper Nanoparticles Obtained by Laser Ablation. *J. Phys. Chem. C* **2011**, *115*, 5021–5027.

(21) Kawamura, G.; Alvarez, S.; Stewart, I. E.; Catenacci, M.; Chen, Z.; Ha, Y. C. Production of Oxidation-Resistant Cu-Based Nanoparticles by Wire Explosion. *Sci. Rep.* **2015**, *5*, 1–8.

(22) Wang, Y.; Asefa, T. Poly(Allylamine)-Stabilized Colloidal Copper Nanoparticles: Synthesis, Morphology, and their Surface-Enhanced Raman Scattering Properties. *Langmuir* **2010**, *26*, 7469–7474.

(23) Pastoriza-Santos, I.; Sánchez-Iglesias, A.; Rodríguez-González, B.; Liz-Marzán, L. M. Aerobic Synthesis of Cu Nanoplates with Intense Plasmon Resonances. *Small* **2009**, *5*, 440–443.

(24) Deng, D.; Jin, Y.; Cheng, Y.; Qi, T.; Xiao, F. Copper Nanoparticles: Aqueous Phase Synthesis and Conductive Films Fabrication at Low Sintering Temperature. *ACS Appl. Mater. Interfaces* **2013**, *5*, 3839–3846.

(25) Chatterjee, A. K.; Sarkar, R. K.; Chattopadhyay, A. P.; Aich, P.; Chakraborty, R.; Basu, T. A Simple Robust Method for Synthesis of Metallic Copper Nanoparticles of High Antibacterial Potency Against E. Coli. *Nanotechnology* **2012**, *23*.

(26) Kamikoriyama, Y.; Imamura, H.; Muramatsu, A.; Kanie, K. Ambient Aqueous-Phase Synthesis of Copper Nanoparticles and Nanopastes with Low-Temperature Sintering and Ultra-High Bonding Abilities. *Sci. Rep.* **2019**, *9*.

(27) Prucek, R.; Kvítek, L.; Panáek, A.; Vanurová, L.; Soukupová, J.; Janík, D.; Zboil, R. Polyacrylate-Assisted Synthesis of Stable Copper Nanoparticles and Copper(I) Oxide Nanocubes with High Catalytic Efficiency. *J. Mater. Chem.* **2009**, *19*, 8463–8469.

(28) Rittermeier, A.; Miao, S.; Schröter, M. K.; Zhang, X.; van den Berg, M. W. E.; Kundu, S.; Wang, Y.; Schimpf, S.; Löffler, E.; Fischer, R. A. et al. The Formation of Colloidal Copper Nanoparticles Stabilized by Zinc Stearate: One-Pot Single-Step Synthesis and Characterization of the Core–Shell Particles. *Phys. Chem. Chem. Phys.* **2009**, *11*, 8358–8366.

(29) Cure, J.; Glaria, A.; Collière, V.; Fazzini, P.-F. F.; Mlayah, A.; Chaudret, B.; Fau, P. Remarkable Decrease in the Oxidation Rate of Cu Nanocrystals Controlled by Alkylamine Ligands. *J. Phys. Chem. C* **2017**, *121*, 5253–5260.

(30) Dang, T. M. D.; Le, T. T. T.; Fribourg-Blanc, E.; Dang, M. C. Synthesis and Optical Properties of Copper Nanoparticles Prepared by a Chemical Reduction Method. *Adv. Nat. Sci Nanosci. Nanotech.* **2011**, *2*, 015009.

(31) Hokita, Y.; Kanzaki, M.; Sugiyama, T.; Arakawa, R.; Kawasaki, H. High-Concentration Synthesis of Sub-10-nm Copper Nanoparticles for Application to Conductive Nanoinks. *ACS Appl. Mat. Int.* **2015**, *7*, 19382–19389.

(32) Jeong, S.; Lee, S. H.; Jo, Y.; Lee, S. S.; Seo, Y.-H.; Ahn, B. W.; Kim, G.; Jang, G.-E.; Park, J.-U.; Ryu, B.-H. et al. Air-Stable, Surface-Oxide Free Cu Nanoparticles for Highly Conductive Cu Ink and their Application to Printed Graphene Transistors. *J. Mat. Chem. C* **2013**, *1*, 2704–2710.

(33) Sun, X. X.; Zhang, Y.-W. W.; Si, R.; Yan, C.-H. H. Metal (Mn, Co, and Cu) Oxide Nanocrystals from Simple Formate Precursors. *Small* **2005**, *1*, 1081–1086.

(34) Salavati-Niasari, M.; Davar, F. Synthesis of Copper and Copper(I) Oxide Nanoparticles by Thermal Decomposition of a New Precursor. *Mater. Lett.* **2009**, *63*, 441–443.

(35) Salavati-Niasari, M.; Davar, F.; Mir, N. Synthesis and Characterization of Metallic Copper Nanoparticles via Thermal Decomposition. *Polyhedron* **2008**, *27*, 3514–3518.

(36) Betancourt-Galindo, R.; Reyes-Rodriguez, P. Y.; Puente-Urbina, B. A.; Avila-Orta, C. A.; Rodríguez-Fernández, O. S.; Cadenas-Pliego, G.; Lira-Saldivar, R. H.; García-Cerda, L. A. Synthesis of Copper Nanoparticles by Thermal Decomposition and Their Antimicrobial Properties. *J. Nanomater.* **2014**, *2014*, 1–5.

(37) Kim, Y. H.; Lee, D. K.; Jo, B. G.; Jeong, J. H.; Kang, Y. S. Synthesis of Oleate Capped Cu Nanoparticles by Thermal Decomposition. *Colloids Surfaces A Physicochem. Eng. Asp.* **2006**, *284-285*, 364–368.

(38) Bhattacharjee, C. R.; Purkayastha, D. D.; Das, N. Surfactant-Mediated Low-Temperature Synthesis of Phase Pure Multiply Twinned Copper Nanoparticles under Non-Inert Condition via Thermal Decomposition of Copper Malonate. *Mat. Lett.* **2013**, *94*, 108 – 111.

(39) Dai, X.; Xu, W.; Zhang, T.; Wang, T. Self-Reducible Cu Nanoparticles for Conductive Inks. *Ind. Eng. Chem. Res.* **2018**, *57*, 2508–2516.

(40) Oliva-Puigdomènech, A.; De Roo, J.; Kuhs, J.; Detavernier, C.; Martins, J. C.; Hens, Z. Ligand Binding to Copper Nanocrystals : Amines and Carboxylic Acids and the Role of Surface Oxides. *Chem. Mater.* **2019**, *31*, 2058–2067.

(41) Coelho, A. Topas Academic v4.1. 2007.

(42) Smits, F. M. Measurement of Sheet Resistivities with the Four-Point Probe. *Bell Syst. Tech. J.* **1958**, *37*, 711–718.

(43) Galwey, A. K.; Jamieson, D. M.; Brown, M. E. Thermal Deconiposition of Three Crystalline Modifications of Anhydrous Copper(II) Formate. *J. Phys. Chem.* **1974**, 2664–2670.

(44) Shin, D. H.; Woo, S.; Yem, H.; Cha, M.; Cho, S.; Kang, M.; Jeong, S.; Kim, Y.; Kang, K.; Piao, Y. A Self-Reducible and Alcohol-Soluble Copper-Based Metal-Organic

Decomposition Ink for Printed Electronics. *ACS Appl. Mater. Interfaces* **2014**, *6*, 3312–3319.

(45) Marchal, W.; Longo, A.; Briois, V.; Van Hecke, K.; Elen, K.; Van Bael, M. K.; Hardy, A. Understanding the Importance of Cu(I) Intermediates in Self-Reducing Molecular Inks for Flexible Electronics. *Inor. Chem.* **2018**, *57*, 15205–15215.

(46) Zhao, Y.; Zhu, J. J.; Hong, J. M.; Bian, N.; Chen, H. Y. Microwave-Induced Polyol-Process Synthesis of Copper and Copper Oxide Nanocrystals with Controllable Morphology. *Eur. J. Inorg. Chem.* **2004**, *2004*, 4072–4080.

(47) Lignier, P.; Bellabarba, R.; Tooze, R. P. Scalable Strategies for the Synthesis of Well-Defined Copper Metal and Oxide Nanocrystals. *Chem. Soc. Rev.* **2012**, *41*, 1708–1720.

(48) Xia, Y.; Xiong, Y.; Lim, B.; Skrabalak, S. E. Shape-Controlled Synthesis of Metal Nanocrystals: Simple Chemistry Meets Complex Physics? *Angew. Chemie - Int. Ed.* **2009**, *48*, 60–103.

(49) Mourdikoudis, S.; Liz-Marzán, L. M. Oleylamine in Nanoparticle Synthesis. *Chem. Mater.* **2013**, *25*, 1465–1476.

(50) Jianlong, W. Enhancement of Citric Acid Production by Aspergillus Niger Using n-Dodecane as an Oxygen-Vector. **2000**, *35*, 1079–1083.

(51) Tam, S. K.; Fung, K. Y.; Sum, G.; Poon, H.; Ng, K. M. Product Design : Metal Nanoparticle-Based Conductive Inkjet Inks. **2016**, *62*.

(52) Abe, S.; Čapek, R. K.; De Geyter, B.; Hens, Z. Tuning the Postfocused Size of Colloidal Nanocrystals by the Reaction Rate: From Theory to Application. *ACS Nano* **2012**, *6*, 42–53.

(53) Abe, S.; Capek, R. K.; De Geyter, B.; Hens, Z. Reaction Chemistry/Nanocrystal Property Relations in the Hot Injection Synthesis, the Role of the Solute Solubility. *ACS Nano* **2013**, *7*, 943–949.

(54) Hens, Z. Economical Routes to Colloidal Nanocrystals. *Science (80-.).* **2015**, *348*, 1211–1212.

(55) Oh, S.-J.; Jo, Y.; Lee, E. J.; Lee, S. S.; Kang, Y. H.; Jeon, H.-J.; Cho, S. Y.; Park, J.-S.; Seo, Y.-H.; Ryu, B.-H. et al. Ambient Atmosphere-Processable, Printable Cu Electrodes for Flexible Device Applications: Structural Welding on a Millisecond Timescale of Surface Oxide-Free Cu Nanoparticles. *Nanoscale* **2015**, *7*, 3997–4004.

(56) Paglia, F.; Vak, D.; van Embden, J.; Chesman, A. S. R.; Martucci, A.; Jasieniak, J. J.; Della Gaspera, E. Photonic Sintering of Copper through the Controlled Reduction of Printed CuO Nanocrystals. *ACS Appl. Mat. Inf.* **2015**, *7*, 25473–25478.

(57) Li, W.; Zhang, H.; Gao, Y.; Jiu, J.; Li, C.-F.; Chen, C.; Hu, D.; Goya, Y.; Wang, Y.; Koga, H. et al. Highly Reliable and Highly Conductive Submicron Cu Particle Patterns Fabricated by Low Temperature Heat-Welding and Subsequent Flash Light Sinter-Reinforcement. *J. Mat. Chem. C* **2017**, *5*, 1155–1164.

(58) Park, B. K.; Kim, D.; Jeong, S.; Moon, J.; Kim, J. S. Direct writing of copper conductive patterns by ink-jet printing. *Thin Solid Films* **2007**, *515*, 7706–7711.

(59) Liu, Y.; Zhang, W.; Yu, H.; Jing, Z.; Song, Z.; Wang, S. A concise and antioxidative method to prepare copper conductive inks in a two-phase water/xylene system for printed electronics. *Chem. Phys. Lett.* **2018**, *708*, 28–31.